

Dynamic stress concentrations around a single fiber break in unidirectional composites: a 3D finite element analysis

Mutlu Caglar^{a*}, Sabuncuoglu Baris^b, Kadioglu F. Suat^a, Swolfs Yentl^c

^aMechanical Engineering Department, Middle East Technical University, Dumlupinar Bulvari 1/6-133, 06800 Çankaya, Ankara, Turkey

^bMechanical Engineering Department, Hacettepe University, Beytepe Campus 06800 Çankaya, Ankara, Turkey

^cDepartment of Materials Engineering, KU Leuven, Kasteelpark Arenberg 44 box 2450, 3001 Leuven, Belgium

Abstract

When a fiber break occurs in longitudinal tension of a unidirectional composite, dynamic stress concentrations arise, which can be different from the ones found considering only static loading. The current paper analyses the dynamic stress concentration factors (SCF) around a fiber break in unidirectional carbon fiber/epoxy composites. 3D finite element models with random and hexagonal fiber distributions were analyzed to investigate the evolution of stress concentrations as a function of time and position. The results indicate that dynamic effects result in much higher SCFs with a larger effective area around the broken fiber. The increase of SCFs in the closest fibers was determined to be larger for lower fiber volume fractions due to the presence of dynamic effects. Similar to the static case, a lower volume fraction causes higher maximum dynamic SCF in random packings. Results also support the high prevalence of coplanar cluster breaks observed in the experiments.

Keywords: Carbon fiber; Polymer-matrix composites (PMCs); Finite element analysis (FEA); Dynamic stress concentrations; Fiber distribution

1. Introduction

Multidirectional fiber-reinforced composites often fail when the 0° plies fail. Studying and thoroughly understanding longitudinal tensile failure is, therefore, crucial in advancing our overall understanding and predictive abilities for many composite applications. Longitudinal tensile failure has received extensive attention in the past, and two benchmarking exercises have been organized in recent years^{1,2}. Even though some models were successful in predicting the longitudinal tensile strength in some cases, this was likely more a coincidence than a sign of true predictive abilities. When the experimental validation is performed based on actual micromechanisms, meaning fiber break and cluster development, then all models show strong discrepancies with experiments^{1,3,4}. These discrepancies have been attributed mainly to the local stress concentrations^{5,6}, dynamic stress concentrations⁶⁻⁸ and issues with the Weibull distribution for fiber strength^{2,9,10}. A particularly important discrepancy is the higher prevalence of coplanar clusters of fiber breaks in the experiments than in model predictions^{3,11,12}. This discrepancy should be largely independent of the Weibull distribution for fiber strength and is, therefore, likely attributed to local or dynamic stress concentrations.

The effect of local stress concentrations was recently investigated for the first time by Yamamoto et al.^{5,13}. In the present study, we focus on the effect of dynamic stress concentrations, which arise immediately after a fiber fractures and releases its stored elastic energy. The conversion from elastic to kinetic energy causes a stress wave to propagate through the broken fiber as well as the nearby intact fibers. When these stress waves dissipate, the system returns to its steady state where the static stress concentrations due to the break exist.

* Corresponding author. Tel.: +90 544 645 95 00

E-mail address: caglarm@metu.edu.tr

The dynamic effect was already included in the very first shear lag model for stress redistribution around fiber breaks by Hedgepeth¹⁴. Hedgepeth reported a static and dynamic SCF of 33% and 53%, respectively, for a 1D packing of fibers. This was reported as a dynamic response factor of $1.53/1.33 = 1.15$, making it seem like a modest increase. However, a dynamic SCF of 53% is 60% higher than the static SCF in relative terms. Hedgepeth and Van Dyke¹⁵ later expanded the analysis from 1D packings to 2D packings. Both studies, however, only analyzed the stress concentrations in the fiber break plane.

Later, more authors studied dynamic stress concentrations. Sakharova and Ovchinskii¹⁶⁻¹⁸ studied a hexagonal 2D packing and included non-linear matrix behavior. They predicted dynamic SCF values that were about twice as high as the static SCFs, which is significantly higher than the 60% predicted by Hedgepeth. They also showed that the dynamic SCFs are largest when the fiber volume fraction is high^{16, 17}. Ji et al.¹⁹ used a similar approach to analyze how the dynamic stress concentrations evolved along the fiber. They found that the dynamic response factor reduced from 1.15 to 1.10 along the fiber. Such a decrease would contribute to explaining the higher prevalence of coplanar fiber break clusters.

Accorsi et al.²⁰ developed the first finite element model for dynamic stress concentration in a 1D packing. They found dynamic response factors ranging from 1.02 to 1.15. They went a step further than previous analyses by also studying the increase in failure probability. This revealed an increase in failure probability ranging from 17% to 40% in the fiber break plane. This could help to explain the discrepancy related to the coplanarity of clusters. Ganesh et al.^{21, 22} recently developed a similar approach that used a plane-strain finite element model with a 1D packing. They also included interfacial debonding, showing that more interface debonding led to lower dynamic SCFs. They used a linear elastic-perfectly plastic matrix behavior with varying tensile yield stress values. For the higher yield stress values (200-270 MPa), the dynamic SCF profiles seemed to reach an equilibrium, but this was primarily attributed to the fact that debonding occurred. In any case, the relevance of including matrix plasticity is questionable, as the very high strain rates are likely to prevent significant yielding^{23, 24}.

More recent developments enabled predicting the effect of dynamic stress concentrations on longitudinal tensile strength^{7, 8, 25}. Bullegas et al.²⁵ temporarily doubled the static SCF values to represent the dynamic effects. Guerrero et al.⁸ studied the effect of the ratio of dynamic over static SCF on strength predictions. Both studies, however, applied the same ratio over the entire stress recovery length. This contradicts the predictions of Ji et al.¹⁹ and Accorsi et al.²⁰, who observed a significant evolution of this factor along the fiber length. Despite the inconsistency, both Bullegas et al. and Guerrero et al. predicted only minor strength reductions even for the highest possible dynamic response factor. This may be attributed to the perfectly plastic behavior used for the matrix in both studies.

Tavares et al.⁷ extended the spring element model of Okabe et al.²⁶ to capture dynamic stress concentrations. They were able to capture the evolution of dynamic stress concentrations along the fiber length. This is, therefore, a powerful approach to capture the dynamic effects in a strength model in a 2D packing, as this model predicts fiber break and cluster development as well. However, it remains questionable how suitable this approach is for dynamic simulations, as (1) the fiber springs are 1D elements and (2) the shear spring stiffness was tuned to capture static stress recovery rather than dynamic stress waves. Thus, they might not correctly capture the stress wave propagation. Nevertheless, the effects that Tavares et al.⁷ reported were in line with data reported in the literature, both in terms of strength and dynamic stress concentrations. In another study, Tavares et al.²⁷ also developed a full finite element model to simulate longitudinal tensile failure, including dynamic effects. However, their model was not used to investigate dynamic stress concentrations. In addition, its current implementation likely had both a too rough mesh and insufficient time resolution to investigate stress concentrations accurately. In a recent study, Barzegar et al.²⁸ modeled the progressive failure and recoil of a fiber using the finite element method. The SCFs were analyzed in the break plane during the fiber failure process. Although they used a powerful approach and investigated the effects of some microstructural parameters in detail, the time resolution was too coarse to capture the dynamic effects after fiber break, which resulted in an underestimation of maximum dynamic SCFs.

Dynamic stress concentrations are observed at timescales of 50 nanoseconds or less, which is out of reach for current experimental characterization techniques²¹. Therefore, this effect should be investigated via analytical or computational models. In the present study, we investigate the stress

concentrations around a fiber break in unidirectional carbon fiber-reinforced composites considering the dynamic effects via a finite element model. This is the first time a 3D finite element model with 2D random fiber packing was used to analyze the dynamic stress concentrations in the entire UD composite considering their evolution over time with sufficient time resolution. To aid the interpretation, the results are always compared to the SCFs obtained for static loading.

2. Model development and analysis procedure

3D unidirectional composite models were generated by following the same procedure in^{29, 30} using the finite element analysis software Abaqus 2020. However, to observe the effect of regular fiber packings and eliminate the complexities introduced by random fiber packings, models with hexagonal fiber packing were also generated and analyzed. Embedded in an epoxy matrix, unidirectional carbon fibers with a 3.5 μm fiber radius (R) were randomly positioned. The center coordinates of the fibers were generated by the algorithm of Melro et al.³¹. The fibers were distributed in a cylindrical representative volume element (RVE) with $36R$ diameter and $120R$ length. Hexagonally distributed fibers were generated with the code used in Sabuncuoglu³² according to the desired fiber volume fraction (V_f). Figure 1a and b present the geometry of the RVE with 50% V_f for randomly and hexagonally distributed intact fibers, respectively. One of the fibers is intentionally positioned at the center of the RVE. This fiber represents the broken fiber in the RVE.

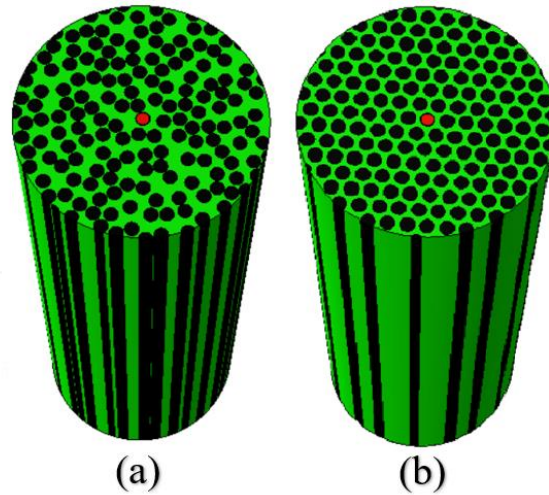


Figure 1. RVE for: (a) random, and (b) hexagonal fiber distribution.

Transversely isotropic elastic material behavior was assigned to the carbon fibers²⁹. In contrast with some of the literature^{7, 22, 27}, we defined the matrix behavior as elastic²⁹. This is more realistic, as the polymer matrix will have insufficient time to yield at the high stress wave speeds occurring after a fiber break^{23, 24}. Table 1 summarizes the properties of both materials. The models do not include fiber-matrix debonding.

Table 1. Material properties of carbon fiber and epoxy²⁹.

Material	Properties									
Carbon fiber	E_{11}	E_{22}	E_{33}	G_{12}	G_{13}	G_{23}	ν_{12}	ν_{13}	ν_{23}	ρ
	230	15	15	13.7	13.7	6	0.25	0.25	0.25	1800
Epoxy	E	ν	ρ							
	3	0.4	1250							

* Modulus and density (ρ) units are GPa and kg/m^3 , respectively.

The analyses were split into two parts for computational efficiency: static and dynamic. In the static step, the material was loaded up to the desired strain without any broken fiber. Considering the length of the model ($L = 120R$), the entire top plane (the farthest plane from the break plane) was displaced by a value corresponding to 0.1% applied strain. For larger strain values, the matrix elements just near

the broken fiber were distorted excessively in the dynamic step, leading to huge errors in the results. Trial analyses with applied strain smaller than 0.1% did not reveal a difference; thus, this strain value was considered appropriate for the analysis. At this step, the lateral boundaries were traction free. Symmetric boundary conditions were applied to the entire bottom plane, which is the break plane. Thus, displacement in the fiber direction (z-axis) and rotations with respect to radial axes (x- and y-axes) were prevented for the nodes at bottom surface. After completing the static step in Abaqus/Standard, the deformed configuration and related material state of the model were transferred to the beginning of the dynamic step ($t = 0$) in Abaqus/Explicit. Initial displacements were automatically specified as being equal to those at the end of static step. In the dynamic step, the top plane displacement in fiber direction was kept fixed while applying symmetric boundary conditions to bottom plane except the middle fiber and maintaining lateral boundaries traction free. At this point, the displacement constraint on the bottom plane of the central fiber was released and the central fiber became traction free on bottom plane in accordance with the improved strategy described in Swolfs et al.³³. This action simulated a fiber break, and the stress state on the whole material changed over time due to stress waves spreading through the material. It should be noted that symmetric boundary conditions were applied to matrix element nodes adjacent to the perimeter of the middle fiber, which was suggested to represent a fiber break more realistically³³. The loading and boundary conditions of static and dynamic steps are shown in Figure 2 and

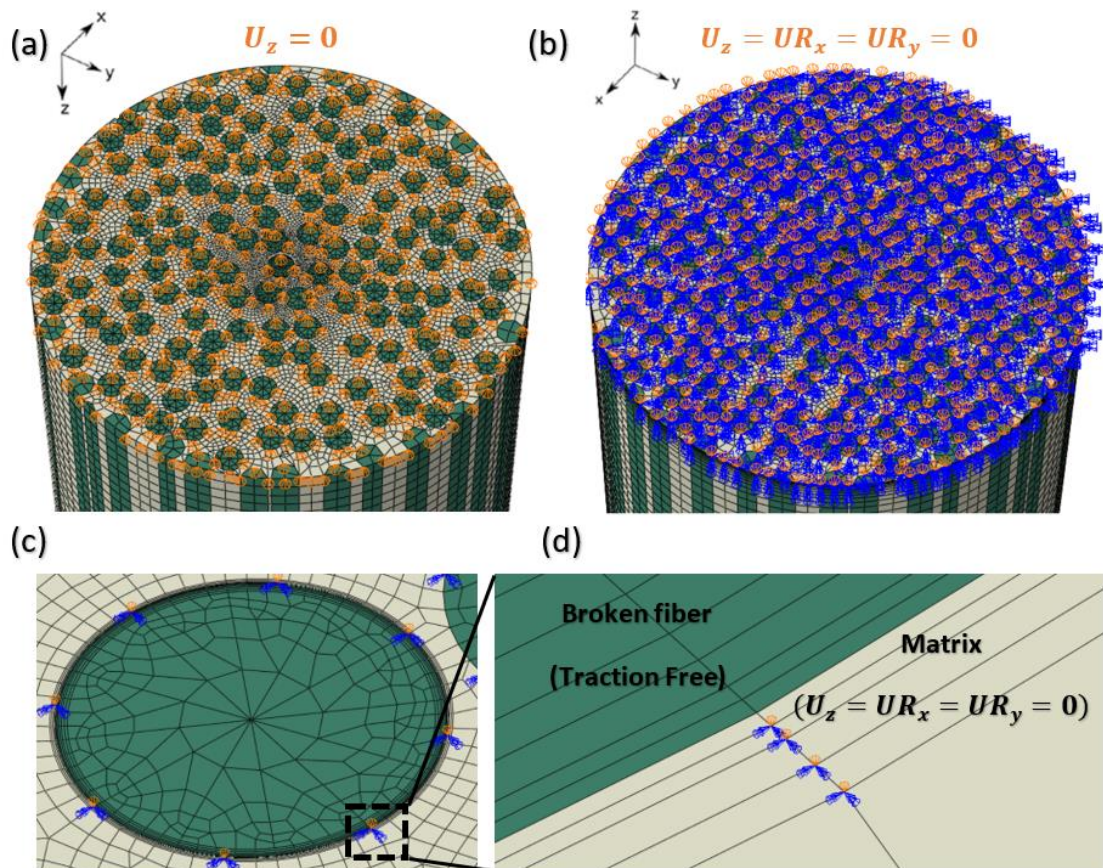


Figure 3, respectively. Mass scaling technique was not used in the dynamic step due to the reasonable computational times, which were around 2 hours for a computer with 16 GB RAM and 8 processors having a clock frequency of 4.5 GHz and 4 cores.

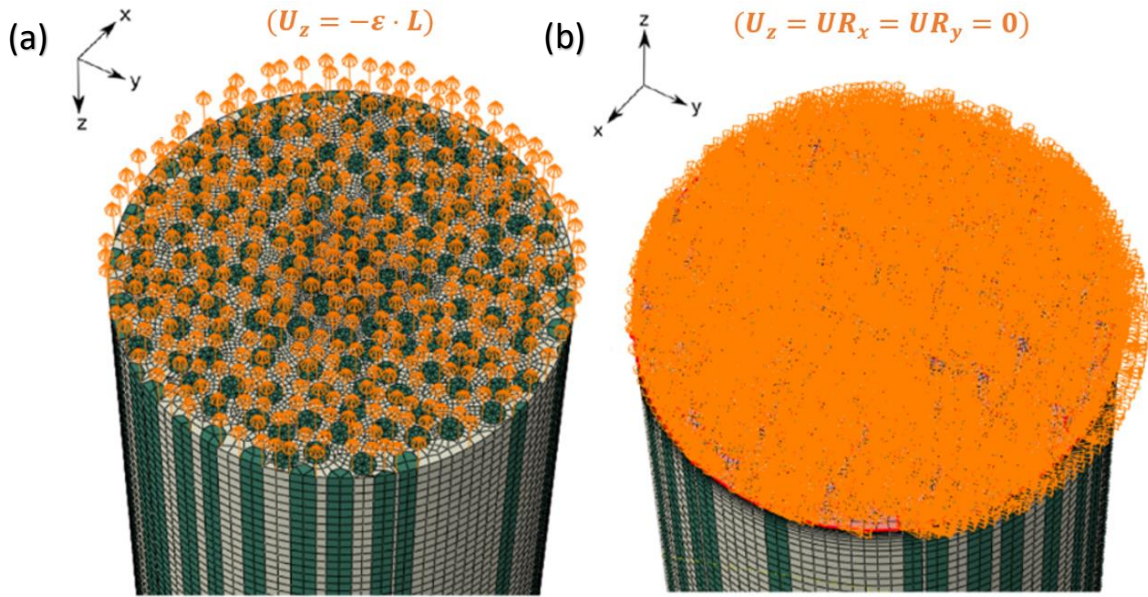


Figure 2. Loading and boundary conditions of the static step on: (a) top plane, and (b) bottom plane.

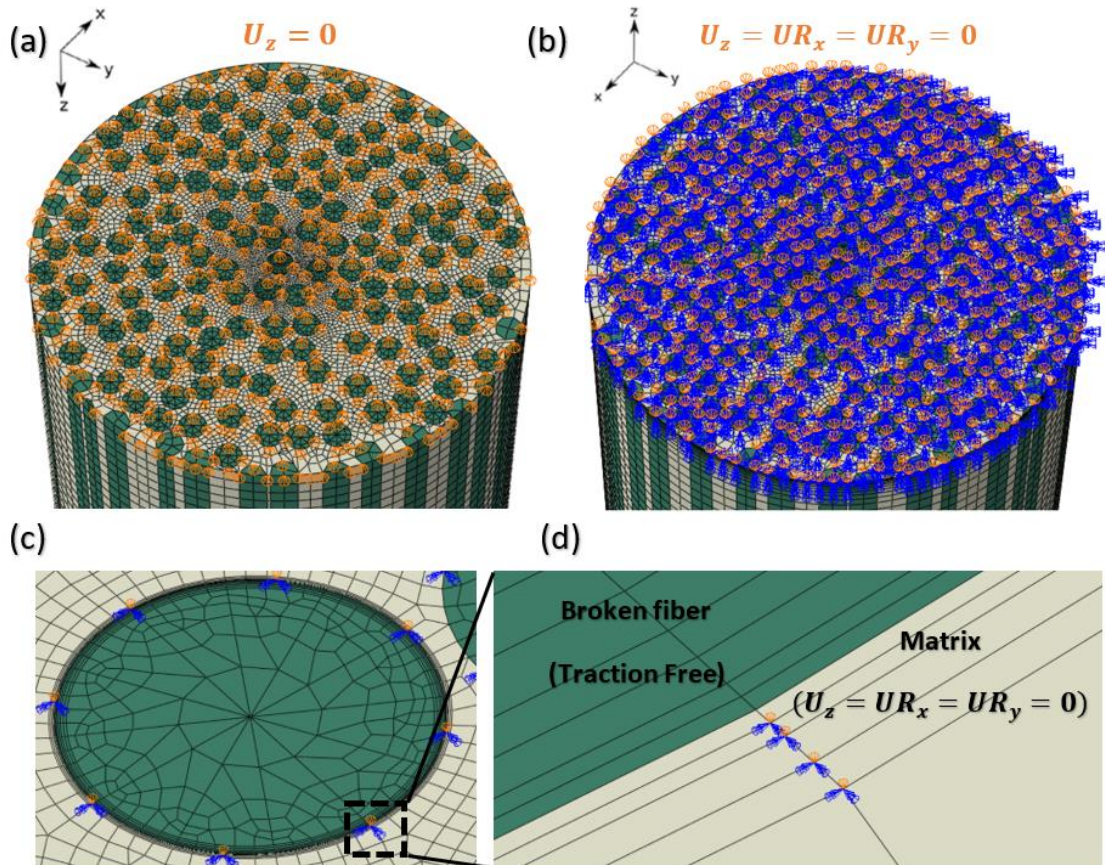


Figure 3. Loading and boundary conditions of the dynamic step: (a) top plane, (b) bottom plane, (c) close-up of the broken fiber on bottom plane, and (d) close-up of the interface region of the broken fiber.

Considering the dynamic SCF results of five fibers closest to the broken fiber, a mesh optimization study was performed both in the longitudinal and the radial direction as in³⁰. For the optimized element sizes, models are divided into 112 planes in the longitudinal direction with smaller element lengths near the break plane (bottom plane), and each model contains over 1 million elements with 75-85% and 15-25% linear brick and wedge elements, respectively. Figure 2 and

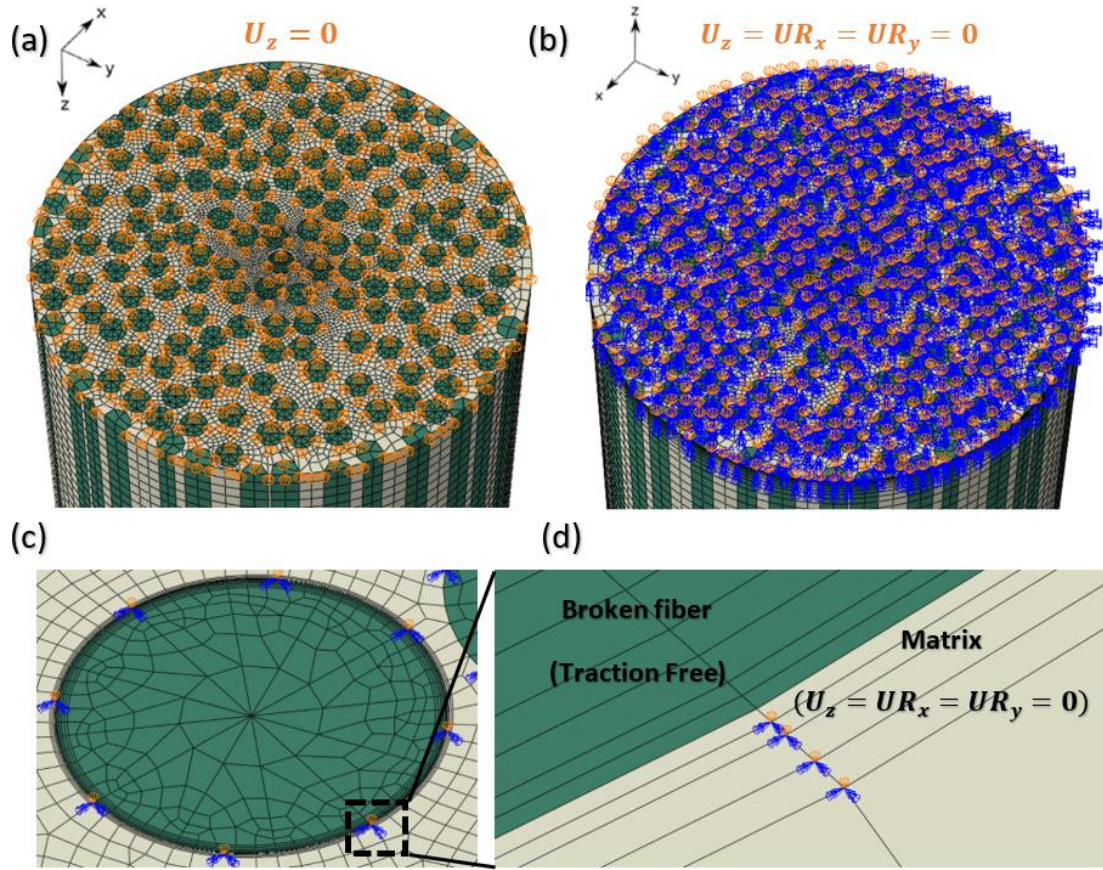


Figure 3 show the radial mesh structure.

Models were generated with 70%, 50% and 30% V_f to investigate its influence on the results. Models consist of 249, 166 and 107 fibers, respectively, including the partial fibers at the boundaries. Although stresses are larger on elements closer to the broken fiber, stresses on each plane of each fiber were calculated by averaging the element stresses on corresponding cross-sections for the same reasons explained in^{29, 34}. Firstly, the failure probability of small volumes would be lower due to the higher Weibull strength. Also, the possibility of using stress concentration results in a strength model in the future makes the average stresses more relevant. By using this average stress concept, the stress concentration factor at a particular plane, z^* , of an individual fiber is calculated by the following equation given in²⁹:

$$SCF_{avg}(z = z^*) = \frac{\sigma_{z,avg}(z = z^*) - \sigma_{z,avg}(z = L)}{\sigma_{z,avg}(z = L)} * 100\% \quad (1)$$

where $\sigma_{z,avg}(z = L)$ is the cross-sectional average stress of that fiber on the plane farthest from the break plane. As the stress state in the material changes over time, SCFs in the dynamic step were calculated for each increment using $\sigma_{z,avg}(z = z^*)$ and $\sigma_{z,avg}(z = L)$ values at the corresponding increment.

Six different models were prepared to examine the effect of parameters on the dynamic behavior (see Table 2). Names of the models were defined according to the packing types and V_f . For example, "Rand50" represents a random fiber distribution with 50% V_f , whereas "Hex70" represents hexagonally distributed fibers with 70% V_f . The model "Rand50" was used as the benchmark model to examine the dynamic SCF and its effects on the composite compared to the static model. The remaining models were used to investigate the effect of V_f and the distribution type on dynamic SCF. In addition, static analyses with a broken fiber were performed to obtain static SCF results of these models to observe the difference.

Table 2. Properties of finite element models.

Model name	Rand30	Rand50	Rand70	Hex30	Hex50	Hex70
Packing type	Random	Random	Random	Hexagonal	Hexagonal	Hexagonal
V_f [%]	30	50	70	30	50	70

3. Results and discussions

3.1. Dynamic response analysis

Initially, the stresses due to fiber fracture were analyzed for the fibers closest to the broken fiber. Fibers were numbered according to their distance from the broken fiber (Figure 4).

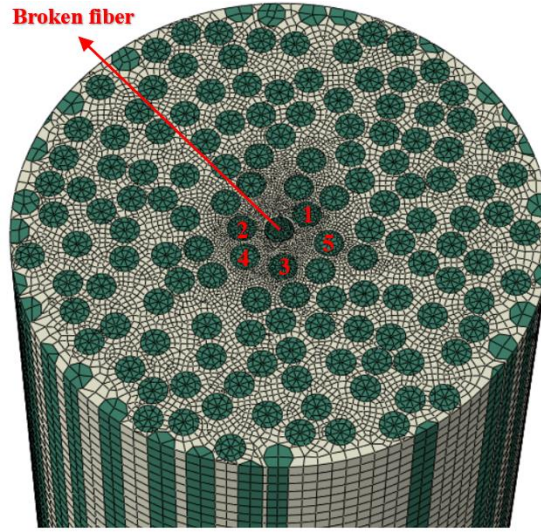


Figure 4. Positions of the broken fiber and the five fibers closest to the broken fiber in Rand50.

Figure 5a presents the stress variation on the broken fiber's top plane (the opposite side of the break plane) with 2 ns time increments for model "Rand50". Approximately at 40 ns, stresses start to deviate remarkably, meaning that the stress wave generated on the bottom plane reaches the top plane. This duration for the stress wave to reach the top plane can also be estimated by the following calculations:

Longitudinal wave speed in carbon fiber (C):

$$C = \sqrt{\frac{E}{\rho}} = \sqrt{\frac{230 \cdot 10^9 \text{ Pa}}{1800 \frac{\text{kg}}{\text{m}^3}}} = 11304 \frac{\text{m}}{\text{s}} = 11304 \cdot 10^6 \frac{\mu\text{m}}{\text{s}} \quad (2)$$

Distance between bottom and top planes (z):

$$z = 120 \cdot R = 120 \cdot 3.5 \mu\text{m} = 420 \mu\text{m} \quad (3)$$

Duration for stress wave to reach the top plane (t):

$$t = \frac{z}{C} = \frac{420 \mu\text{m}}{11304 \cdot 10^6 \frac{\mu\text{m}}{\text{s}}} = 3.72 \cdot 10^{-8} \text{ s} = 37.2 \text{ ns} \quad (4)$$

This calculated value of t is close to the 40 ns determined from the analysis, confirming the accuracy of the analysis. In Figure 5b, the stress variation in the break plane is presented for a fiber near the

lateral boundary of the model with 0.5 ns increments. The magnitude of the stress starts to deviate remarkably around 30 ns, which means that the stress wave reaches the lateral boundary around this time. Therefore, all remaining dynamic SCF results are presented up to 30 ns with 0.5 ns time increments for more accurate results. Thus, the RVE dimensions (36R diameter, 120R length) are large enough for the results to be unaffected by the model size.

Figure 6 reveals the variations of maximum dynamic SCFs of the five closest fibers in model “Rand50” (see Figure 4 for the packing). Each indicator represents the maximum value along the corresponding fiber at the specified time. Note that these maximum values were extracted from either the break plane or near the break plane ($z/L < 2\%$). Moreover, the maximum dynamic SCFs of these fibers obtained in the entire time interval are presented in Table 3, together with the ratio of the radial distance of the corresponding fiber over the fiber radius (d/R), maximum static SCF and ratio of dynamic to static SCF (defined as max SCF ratio). Note that d is the radial distance between the surfaces of the broken fiber and the fiber that was analyzed. Results show that the dynamic case creates much larger SCFs than the static case. This results in a much higher failure probability of the intact fibers and, accordingly, would reduce the predicted strength properties for a unidirectional composite.

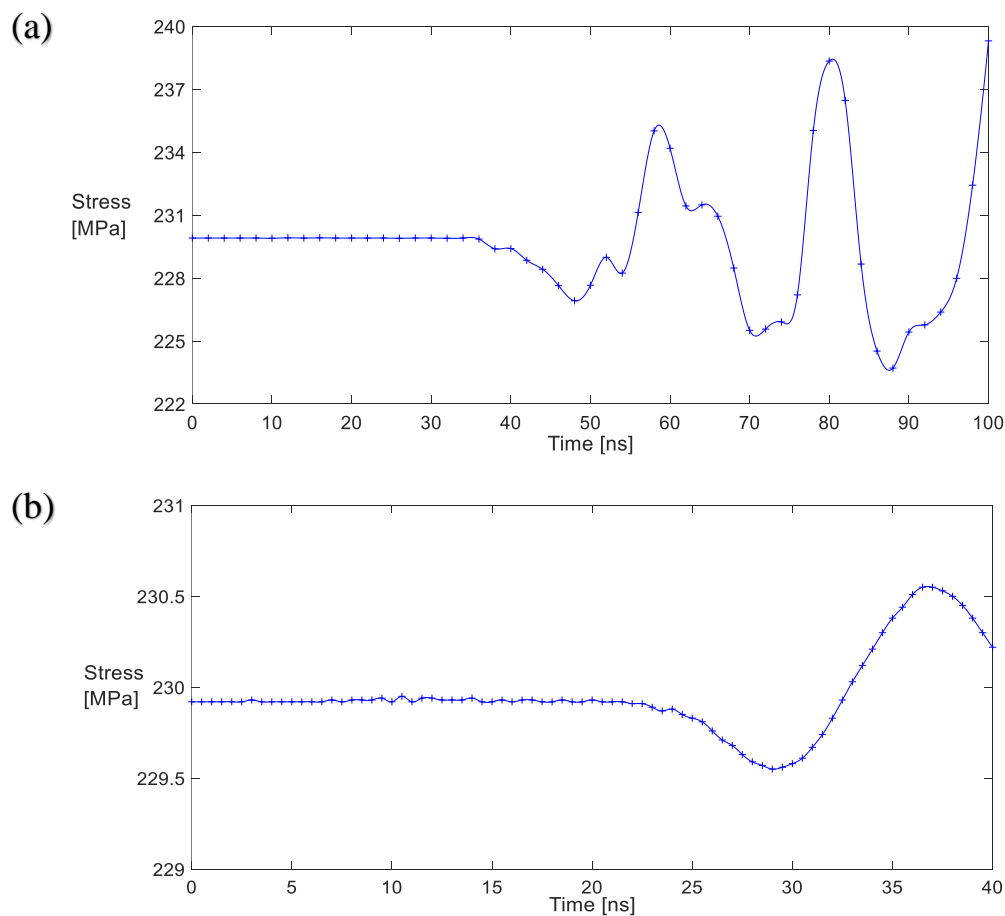


Figure 5. Stress variations in the “Rand50” model: (a) on the top plane (opposite side of the break plane) for the fiber closest to the broken fiber, and (b) on the break plane for a fiber near the lateral boundary of the model

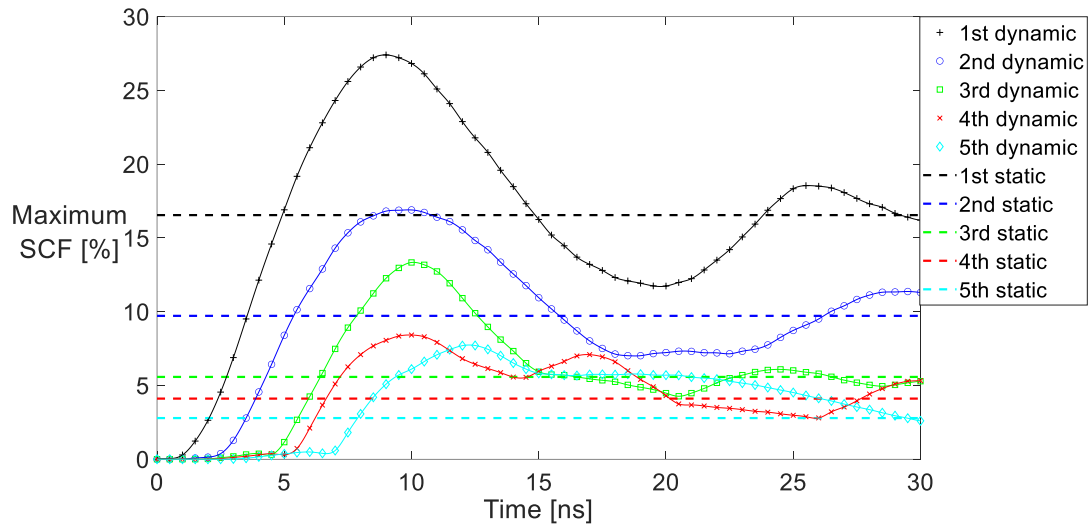


Figure 6. Variation of maximum dynamic SCFs obtained along the closest 5 fibers. The static SCF values are included as straight, dashed lines to facilitate the comparison.

Figure 6 reveals that the dynamic SCFs start to increase earlier for closer fibers as their radial distance to the broken fiber is smaller. For each fiber, the dynamic SCF reaches a maximum value and then fluctuates around the corresponding static one. As the closest two fibers are much closer than the 3rd, 4th, and 5th ones, SCFs are concentrated on these two fibers for both static and dynamic cases. However, the 3rd, 4th, and 5th closest fibers have a higher maximum SCF ratio than the two closest fibers (see Table 3). This indicates that the importance of the dynamic effects is more significant for the 3rd, 4th, and 5th closest fibers, at least in relative terms to the static case. The dynamic SCFs on these fibers are so high (13.3%, 8.4% and 7.7%, respectively) that they are close to the static SCFs of the two closest fibers.

Table 3. Maximum SCF results of the closest five fibers

Fiber	1st	2nd	3rd	4th	5th
d/R	0.18	0.48	0.93	1.10	1.50
Max. dynamic SCF [%]	27.4	16.9	13.3	8.4	7.7
Max. static SCF [%]	16.6	9.7	5.6	4.1	2.8
Max SCF ratio	1.66	1.74	2.39	2.05	2.76

The early works on dynamic SCF^{14, 15} also used the max. SCF ratio, albeit using $(1+SCF)$ in calculating the ratio. This ratio may give the impression that the dynamic stress concentrations are more severe on fibers farther away from the broken fiber. However, both the dynamic and static SCFs on those fibers are significantly smaller and hence less relevant for the composite strength. It is therefore also useful to compare how the maximum SCF ratio and the maximum SCF difference depend on d/R , as presented in Figure 7a and Figure 7b, respectively. The maximum SCF difference is the difference between the maximum dynamic and static SCFs. For the closest two fibers, the dynamic to static SCF ratios are close to 2 (see Table 3), and the differences between them are relatively high (see Figure 7b). Even the 3rd closest fiber has both a high SCF ratio and a high SCF difference. Therefore, the presence of dynamic effects puts these fibers in a more critical condition.

Figure 7b reveals that the maximum SCF difference has a decreasing trend with radial distance, as both dynamic and static SCF results are smaller for fibers farther from the broken fiber. Despite the decreasing trend in maximum SCF difference, the maximum SCF ratio is higher for fibers farther away from the broken fiber. This shows that such fibers are affected more by the dynamic effects in relative terms (see Figure 7a) but not in absolute terms (see Figure 7b). Therefore, the maximum SCF ratio

values previously reported in the literature should be interpreted with care. Because the dynamic effects increase the SCF values more on nearby fibers than fibers farther away (see Figure 7b), the presence of the dynamic effects should increase the localization of clusters rather than delocalizing them. Including dynamic effects in strength models should therefore create more coplanar clusters, bringing them more in line with experimental observations^{3, 35}.

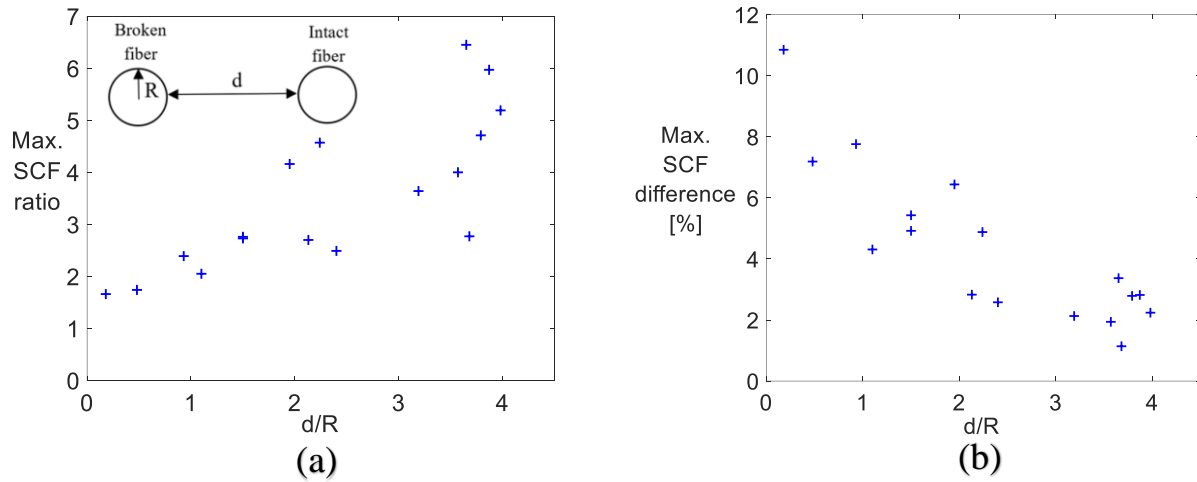


Figure 7. Variation of maximum (a) SCF ratio, and (b) SCF difference with respect to d/R .

Figure 8a presents the variation in maximum SCF ratios along the fiber direction for the closest two fibers. In addition, Figure 8b presents the maximum SCF difference along the closest two fibers. These curves are plotted for the moments the maximum dynamic SCFs are obtained ($t = 9$ ns and $t = 10$ ns for the 1st and 2nd closest fibers, respectively, see Figure 6). Thus, the most critical fibers in the whole material are examined in these figures at their most critical time increments. The maximum SCF ratio reaches its local maxima approximately at $z/R = 9$ and $z/R = 10$ for the 1st and 2nd closest fibers, respectively. This ratio is close to “2” at the break plane. The regions at $z/R = 9$ and $z/R = 10$ seem to be more critical at first sight. However, the SCF difference and dynamic SCF are much larger on break plane and in its neighborhood, which results in a higher probability of a break taking place in the vicinity of these regions. This does not mean the regions around $z/R = 9$ and $z/R = 10$ are not critical, as the dynamic SCF is 10 times higher than the static one for at least two fibers at those axial distances.

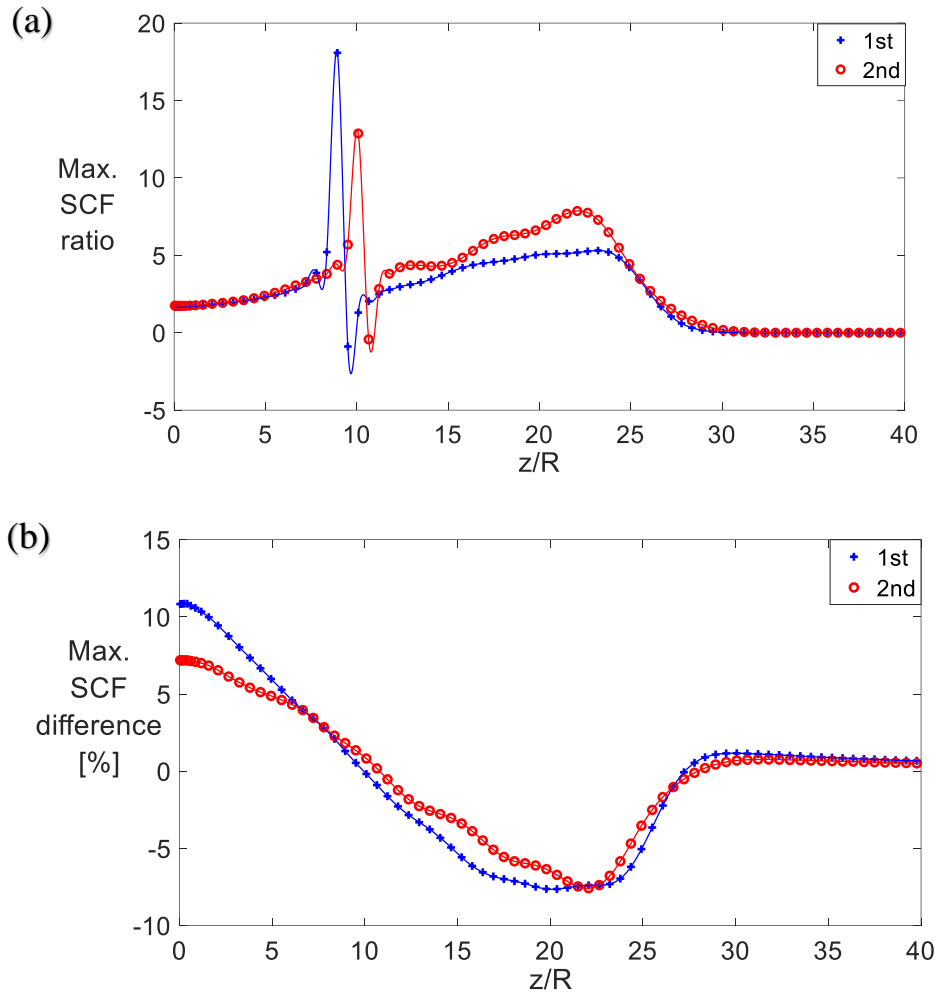


Figure 8. Variation in maximum: (a) SCF ratio, and (b) SCF difference along the fiber axis at $t=9$ ns and $t=10$ ns for the 1st and 2nd closest fibers, respectively.

Two more local maximum values far from the break plane can be seen in Figure 8a (at $z/R = 23$ and $z/R = 22$). The SCF difference is negative in those regions, which means that both dynamic and static SCFs are negative. Therefore, results for these regions can be disregarded and considered not critical at those corresponding times. Note that negative SCF means that the fiber is under tension with a stress level smaller than the nominal level. Such negative SCFs were also reported in the literature^{29, 36}. The rapid decrease in maximum SCF difference in Figure 8b implies that dynamic effects make the development of coplanar clusters more likely. Although not presented, fibers farther away from the broken fiber were also examined, and this rapid decrease in maximum SCF difference was not observed on those fibers. Thus, this effect is localized to the closest fibers only. In addition, the maximum SCF ratio and difference for the closest fiber were examined for other time increments, and the decrease was less sharp than the ones in Figure 8b on the farther planes where dynamic SCFs are significant. Dynamic effects, therefore, make it more likely that the next fiber break will appear near the break plane rather than further away from it. This finding contributes to the experimental observation that coplanar clusters are more common than predicted by state-of-the-art strength models for longitudinal tensile failure that consider only static stress concentrations^{3, 35}.

3.2. Effect of fiber volume fraction

Figure 9 presents the maximum dynamic SCF change in the closest fiber for 30%, 50% and 70% V_f in a random fiber packing. Again, these maximum values were found on the break plane or just near the break plane ($z/L < 0.5\%$). As the radial distance of the closest fiber is smaller for higher V_f , the SCF in the “Rand70” model reaches its peak value sooner than the others. One may expect to find the largest

peak value in the “Rand30” model due to the lack of shielding effect explained in Swolfs et al.²⁹. Packings with a large V_f will tend to have more nearby fibers, which contribute to carrying the SCFs. The d/R values of the closest three fibers in “Rand70” are 0.04, 0.19 and 0.19, which are smaller than the d/R value of the closest fiber in “Rand30” (0.37) (see Figure 10). Therefore, the stress from the broken fiber is shed to more neighboring fibers in “Rand70”, which should result in smaller SCF on the closest fiber in “Rand70” compared to “Rand30”. However, this is not the case in Figure 9. The largest peak value was found in the “Rand70” model. This may be caused by the SCF being inversely proportional to the radial distance of a fiber to the broken fiber because fibers in the “Rand70” model were located closer to the broken fiber than those in the “Rand30” model. This proximity effect and the shielding effect counteract each other. To further illustrate this, two new models with 30% and 50% V_f were created to remove the effect of the radial distance of the closest fiber. The closest fiber in these new models was repositioned to have the same radial distance to the broken fiber as in “Rand70”. The positions of the rest of the fibers were left unchanged.

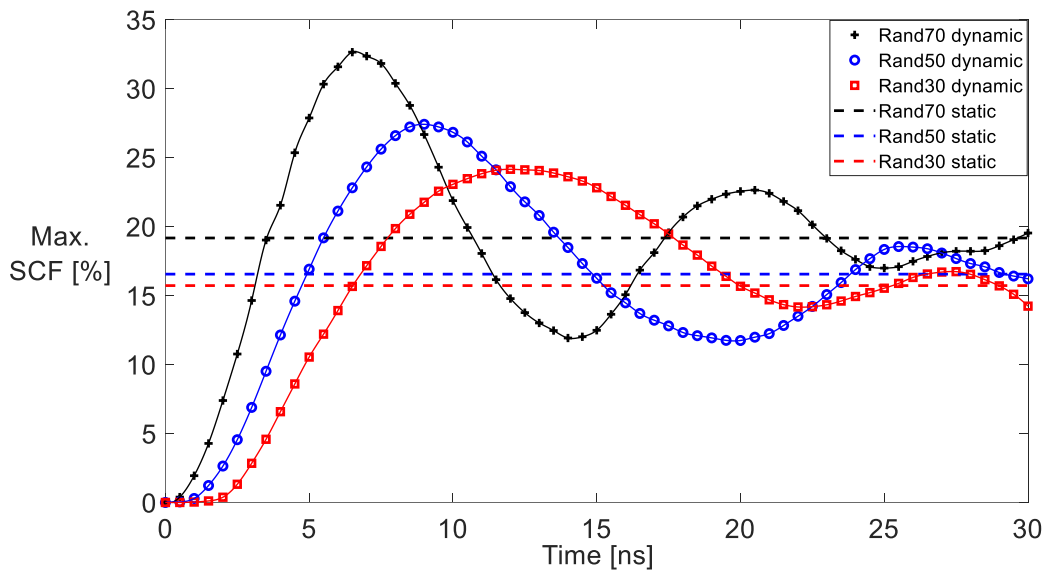


Figure 9. Variation in maximum dynamic SCF of the closest fiber for different fiber volume fractions with random packing.

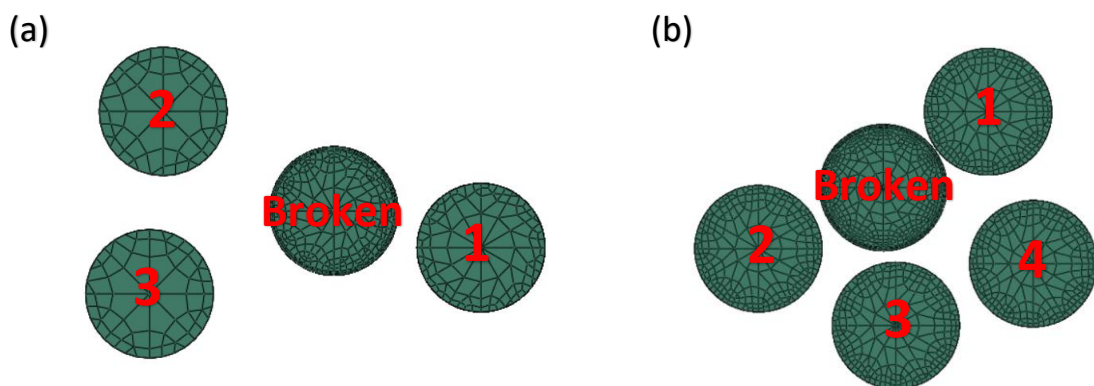


Figure 10. Positions of the fibers closest to the broken fiber: (a) three closest fibers in “Rand30”, and (b) four closest fibers in “Rand70”.

Figure 11 reveals the variation in dynamic SCF of the closest fibers for their new positions. The results were found either on the break plane or just near the break plane ($z/L < 0.1\%$), as those in Figure 9. As the radial distance of the closest fiber to the broken fiber is the same for all models, the dynamic SCFs initially increase similarly in all models. Different from the results in Figure 9, the highest and the lowest peaks were found in “Rand30” and “Rand70”, respectively. This validates the existence of

shielding effect mentioned above: more neighboring fibers share the excess load in higher V_f resulting in lower dynamic and static SCFs. The closest fibers were intentionally placed at the same radial distance in these particular models. Due to the randomness of fiber positions in a real composite, a definite conclusion regarding the effect of V_f on the SCF of the closest fiber cannot be deduced due to the mentioned counteracting effects that take place when V_f changes.

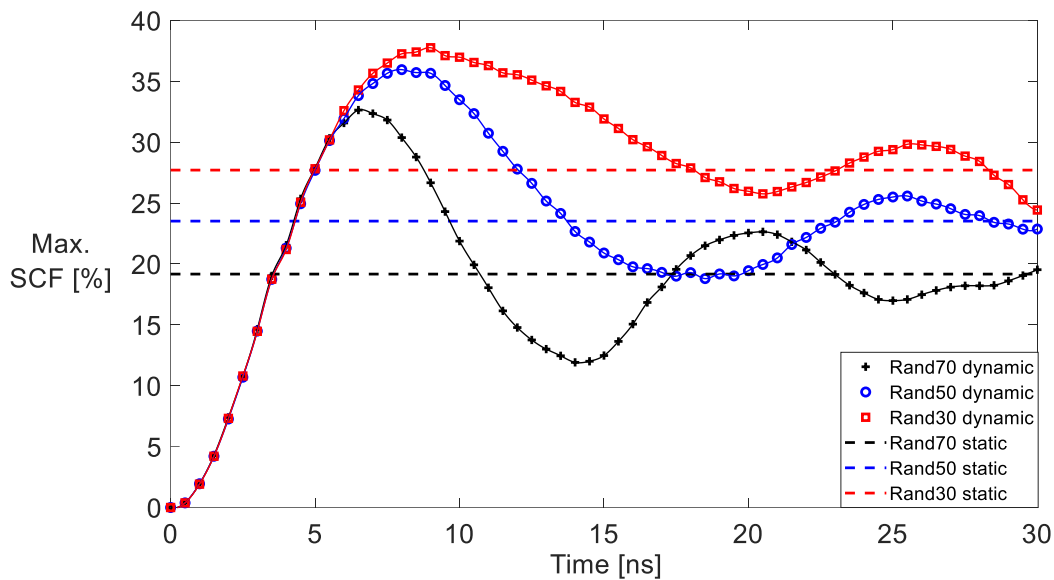


Figure 11. Variation in maximum dynamic SCF of the closest fiber for different fiber volume fractions with modified radial distance in random packing.

In addition to the closest fiber, both dynamic and static SCFs are examined for farther fibers in the original models with 30%, 50% and 70% V_f (Figure 12). Each indicator represents the maximum dynamic and static SCFs found along each fiber during the entire time interval. For both dynamic and static cases, the trend lines are higher for lower V_f . This means that SCFs at the same distances are higher for lower V_f , which is caused by the shielding effect mentioned above. Also, all the results presented up to $d/R = 3$ were found on the break plane or just near the break plane ($z/L < 3\%$), while some of them were found on farther planes for $d/R > 3$. This also justifies the possibility of higher prevalence of coplanar breaks in case of a fiber break.

Maximum dynamic to maximum static SCF ratios and maximum SCF differences of “Rand30”, “Rand50” and “Rand70” are investigated in Figure 13. SCF ratios of the few closest fibers in all three models are close to each other. However, higher V_f results in higher ratios for farther fibers. “Rand50” and “Rand70” models result in larger maximum SCF differences for the closest fibers. However, considering the whole graph, a lower V_f results in higher maximum SCF differences.

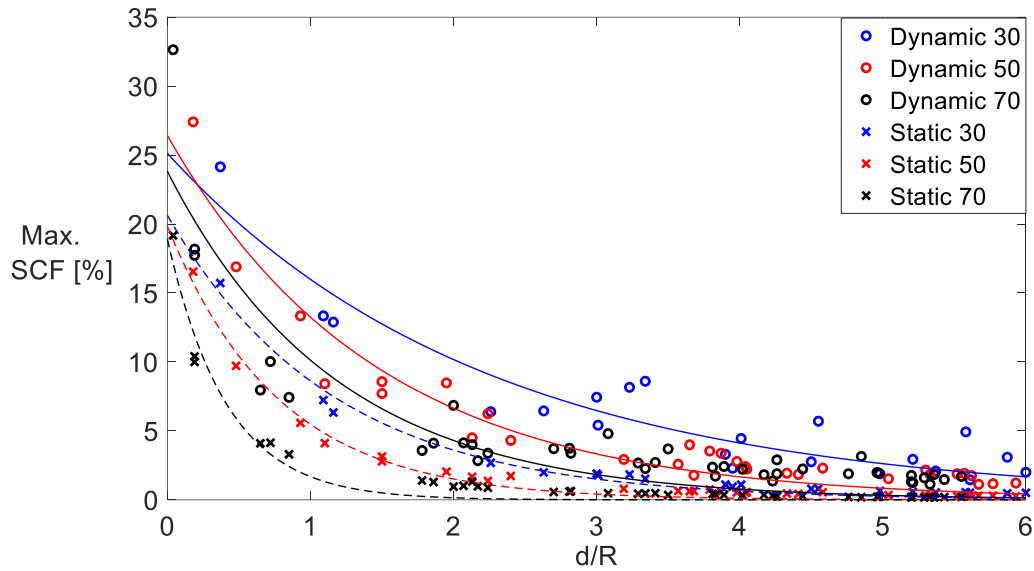


Figure 12: Change in maximum dynamic and static SCFs with d/R for different V_f with randomly distributed fibers.

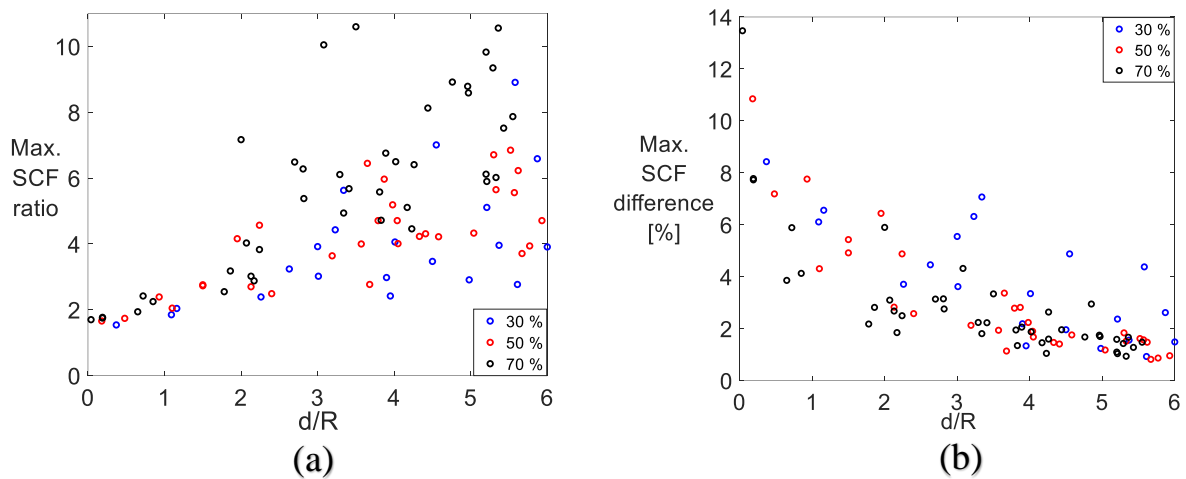


Figure 13: Change in maximum SCF ratios and SCF differences with d/R for different V_f with randomly distributed fibers: (a) maximum SCF ratios, and (b) maximum SCF differences.

Given the inherent variation in random fiber packings, it is not easy to derive strong conclusions from such packings on the effect of V_f . To avoid this random fiber distribution effect, the maximum dynamic SCF results of the closest fiber are analyzed for the models in which the fibers are distributed in a regular hexagonal packing (“Hex30”, “Hex50” and “Hex70”) (Figure 14). In the hexagonal packing, radial distances of the closest six fibers and, therefore, the maximum dynamic SCFs on those fibers are equal in a single RVE. The radial distances of the fibers are coupled with V_f . As there are more fibers in a model with higher V_f , radial distances get smaller with increasing V_f .

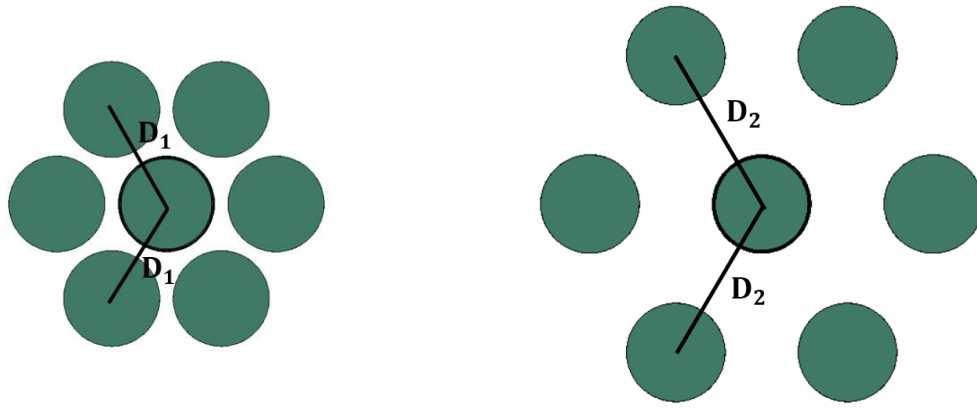


Figure 14: Hexagonal packings with: (a) 70%, and (b) 30% V_f

Figure 15 reveals that the closest fiber in “Hex70” has the largest maximum dynamic SCF, followed by those in “Hex50” and “Hex30”. In this regular distribution of fibers, all the 6 intact nearest fibers are equidistant to broken fiber, regardless of V_f . Therefore, intact fibers are positioned closer to the broken fiber when V_f increases, and the proximity effect is observed. However, the shielding effect cannot be observed since the additional load is always shared by the same number (6) of intact fibers.

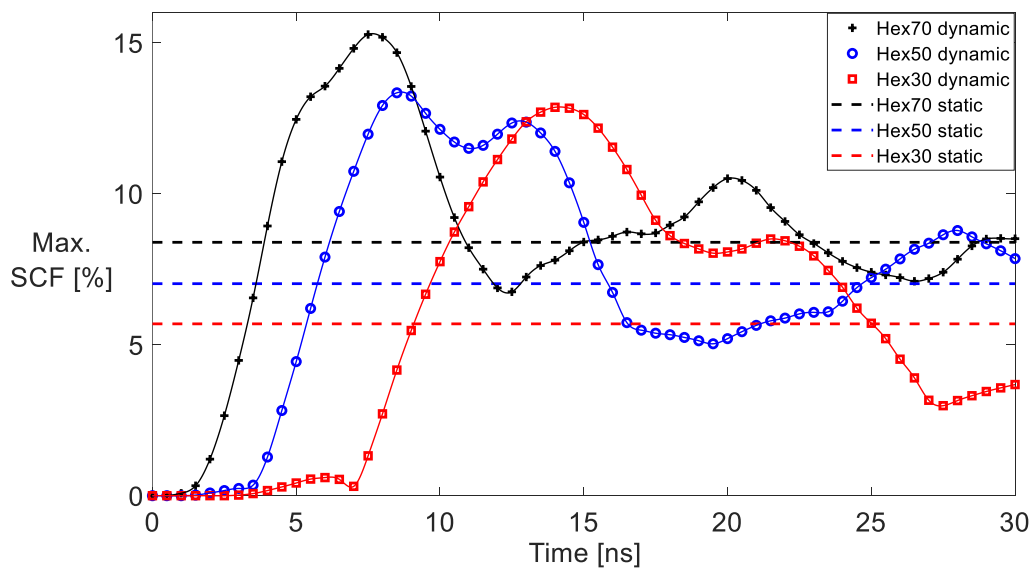


Figure 15. Variation in maximum dynamic SCF of the closest fiber for different fiber volume fractions with hexagonal packing.

As seen in Figure 15, hexagonal fiber distribution resulted in higher peak SCF results for higher V_f as radial distances of the intact fibers are coupled with V_f . However, it is the opposite for random fiber distribution, where counteracting shielding effect becomes dominant (Figure 11). Thus, these results show the importance of using random fiber distribution in computational methods for more accurate SCF results due to the random nature of fiber positions in real microstructures.

4. Conclusion

Stress concentrations in unidirectional carbon-epoxy composites were investigated for the case of a single fiber break, including dynamic effects. These were analyzed for different distributions and fiber volume fractions. The results show that the dynamic effects cause significantly larger SCFs than in static loading. The relative SCF increase in farther fibers is higher, and a larger area around the broken fiber is affected by the fiber break when dynamic effects are included. Considering the SCFs on the

closest fiber at the most critical time increment, the increase in SCF due to dynamic effects was highest near the break plane. This can therefore contribute to explaining the higher prevalence of coplanar clusters observed in experiments versus in models³. Therefore, we suggest that dynamic effects should be considered in longitudinal tensile strength models.

For random fiber distribution, higher V_f resulted in lower maximum SCF, which was shown to be due to the shielding effect caused by the existence of more close fibers contributing to carrying the SCFs in composites with higher V_f . For hexagonal packing, the opposite was obtained due to the smaller radial distance of the closest fiber. Therefore, this study showed that not only the V_f but also the locations of the fibers play a key role in the SCFs on the fibers.

Future work will implement these dynamic stress concentrations in a fiber break model to assess their effect on the strength, cluster development and coplanarity of the clusters.

Data Availability

The raw/processed data required to reproduce these findings can be obtained from the corresponding author upon request.

References

1. Bunsell A, Gorbatikh L, Morton H, et al. Benchmarking of strength models for unidirectional composites under longitudinal tension. *Composites Part A: Applied Science and Manufacturing* 2018; 111: 138-150.
2. Breite C, Melnikov A, Turon A, et al. Blind benchmarking of seven longitudinal tensile failure models for two virtual unidirectional composites. *Composites Science and Technology* 2021; 202: 108555.
3. Swolfs Y, Morton H, Scott AE, et al. Synchrotron radiation computed tomography for experimental validation of a tensile strength model for unidirectional fibre-reinforced composites. *Composites Part A: Applied Science and Manufacturing* 2015; 77: 106-113.
4. Pimenta S. A computationally-efficient hierarchical scaling law to predict damage accumulation in composite fibre-bundles. *Composites Science and Technology* 2017; 146: 210-225.
5. Yamamoto G, Onodera M, Koizumi K, et al. Considering the stress concentration of fiber surfaces in the prediction of the tensile strength of unidirectional carbon fiber-reinforced plastic composites. *Composites Part A: Applied Science and Manufacturing* 2019; 121: 499-509.
6. Swolfs Y, Verpoest I and Gorbatikh L. A review of input data and modelling assumptions in longitudinal strength models for unidirectional fibre-reinforced composites. *Composite Structures* 2016; 150: 153-172.
7. Tavares RP, Otero F, Baiges J, et al. A dynamic spring element model for the prediction of longitudinal failure of polymer composites. *Computational Materials Science* 2019; 160: 42-52.
8. Guerrero JM, Mayugo JA, Costa J, et al. Failure of hybrid composites under longitudinal tension: Influence of dynamic effects and thermal residual stresses. *Composite Structures* 2020; 233: 111732.
9. Swolfs Y, Verpoest I and Gorbatikh L. Issues in strength models for unidirectional fibre-reinforced composites related to Weibull distributions, fibre packings and boundary effects. *Composites Science and Technology* 2015; 114: 42-49.
10. Joannès S, Islam F and Laiarinandrasana L. Uncertainty in fibre strength characterisation due to uncertainty in measurement and sampling randomness. *Applied Composite Materials* 2020; 27: 165-184.

11. Van den Heuvel P, Van der Bruggen Y and Peijs T. The influence of carbon fibre surface treatment on fibre-fibre interactions in multi-fibre microcomposites. *Advanced Composites Letters* 1994; 3: 096369359400300603.
12. Jones KD and DiBenedetto AT. Fiber fracture in hybrid composite systems. *Composites Science and Technology* 1994; 51: 53-62.
13. Yamamoto G, Koizumi K, Nakamura T, et al. Tensile-strength-controlling factors in unidirectional carbon fiber reinforced plastic composites. *Composites Part A: Applied Science and Manufacturing* 2021; 140: 106140.
14. Hedgepeth JM. Stress concentrations in filamentary structures. National Aeronautics and Space Administration, 1961.
15. Hedgepeth JM and Van Dyke P. Local stress concentrations in imperfect filamentary composite materials. *Journal of composite materials* 1967; 1: 294-309.
16. Sakharova E and Ovchinskii A. Influence of dynamic effects accompanying rupture of fibers and separation of fibers from the matrix on interaction between failure micromechanisms of composite materials. *Mechanics of Composite Materials* 1984; 20: 323-327.
17. Sakharova E and Ovchinskii A. Dynamics of stress redistribution in fiber fracture in composites. *Mechanics of Composite Materials* 1981; 16: 417-422.
18. Sakharova E and Ovchinskii A. Dynamics of stress redistribution in a ruptured fiber of a composition material. *Mechanics of Composite Materials* 1979; 15: 45-51.
19. Ji X, Liu X-R and Chou T-W. Dynamic stress concentration factors in unidirectional composites. *Journal of composite materials* 1985; 19: 269-275.
20. Accorsi M, Pegoretti A and Dibenedetto A. Dynamic analysis of fibre breakage in single-and multiple-fibre composites. *Journal of materials science* 1996; 31: 4181-4187.
21. Ganesh R, Sockalingam S, Haque BZ, et al. Dynamic effects of single fiber break in unidirectional glass fiber-reinforced composites. *Journal of Composite Materials* 2017; 51: 1307-1320.
22. Ganesh R, Sockalingam S and Gillespie JW. Dynamic effects of a single fiber break in unidirectional glass fiber-reinforced polymer composites: Effects of matrix plasticity. *Journal of Composite Materials* 2018; 52: 1873-1886.
23. Tamrakar S, Ganesh R, Sockalingam S, et al. Experimental investigation of strain rate and temperature dependent response of an epoxy resin undergoing large deformation. *Journal of Dynamic Behavior of Materials* 2018; 4: 114-128.
24. Tamrakar S, Ganesh R, Sockalingam S, et al. Strain rate-dependent large deformation inelastic behavior of an epoxy resin. *Journal of Composite Materials* 2020; 54: 71-87.
25. Bullegas G, Lamela JM, Pimenta S, et al. On the role of dynamic stress concentrations and fracture mechanics in the longitudinal tensile failure of fibre-reinforced composites. *Engineering Fracture Mechanics* 2020; 228: 106920.
26. Okabe T, Sekine H, Ishii K, et al. Numerical method for failure simulation of unidirectional fiber-reinforced composites with spring element model. *Composites Science and Technology* 2005; 65: 921-933.
27. Tavares RP, Melro AR, Bessa MA, et al. Mechanics of hybrid polymer composites: analytical and computational study. *Computational Mechanics* 2016; 57: 405-421.
28. Barzegar M, Costa J and Lopes CS. High-fidelity computational micromechanics of first-fibre failure in unidirectional composites: Deformation mechanisms and stress concentration factors. *International Journal of Solids and Structures* 2020; 204: 18-33.
29. Swolfs Y, Gorbatikh L, Romanov V, et al. Stress concentrations in an impregnated fibre bundle with random fibre packing. *Composites Science and Technology* 2013; 74: 113-120.
30. Sabuncuoglu B, Mutlu C, Kadioglu FS, et al. Stress redistribution around fiber breaks in unidirectional steel fiber composites considering the nonlinear material behavior. *Composite Structures* 2020; 239: 111959.

31. Melro A, Camanho P and Pinho S. Generation of random distribution of fibres in long-fibre reinforced composites. *Composites Science and Technology* 2008; 68: 2092-2102.
32. Sabuncuoglu B. On the high stress concentrations in steel fiber composites under transverse loading. *Journal of Reinforced Plastics and Composites* 2014; 33: 1941-1953.
33. Swolfs Y, McMeeking RM, Verpoest I, et al. Matrix cracks around fibre breaks and their effect on stress redistribution and failure development in unidirectional composites. *Composites Science and Technology* 2015; 108: 16-22.
34. Swolfs Y, Gorbatikh L and Verpoest I. Stress concentrations in hybrid unidirectional fibre-reinforced composites with random fibre packings. *Composites Science and Technology* 2013; 85: 10-16.
35. Breite C, Melnikov A, Turon A, et al. Detailed experimental validation and benchmarking of six models for longitudinal tensile failure of unidirectional composites. *Composite Structures* 2022; 279: 114828.
36. Nedele MR and Wisnom MR. Three-dimensional finite element analysis of the stress concentration at a single fibre break. *Composites science and technology* 1994; 51: 517-524.